43

NACA0012翼まわりの遷音速流に関する予備研究

アンディ・エカ・サキャ*　中村佳朗*　保原充*

A Preliminary Study of Transonic Flow around NACA0012

by

Andi E. SAKYA, Yoshiaki NAKAMURA
and Michiru YASUHARA
Department of Aeronautical Engineering, Nagoya University

ABSTRACT

A typical transonic flow at $M_\infty = 0.80$ and $Re = 1 \times 10^6$ is numerically simulated by using the Yee-Harten TVD Scheme of Euler Backward Implicit method. This study treats unsteady, inviscid or viscous compressible flows. In the viscous flow case, two turbulence models are applied: Baldwin-Lomax model (BLM) and Stock-Haase model (SHM). Comparison with the experimental data shows a good agreement.

1. INTRODUCTION

The characteristic of aerodynamics in transonic flow regime is of great importance, since in this speed range most civil aircrafts cruise. A typical transonic flow has a subsonic free stream from which the flow accelerates to a supersonic speed along the airfoil surface. The deceleration from supersonic to subsonic flow, in general, passes through a shock wave.

If a shock strength is sufficiently large, a boundary layer separation will occur near the shock. Depending on the airfoil configuration, there may also occur a separation at the trailing edge, that can merge with the shock induced separation region. In that case, the boundary layer is generally turbulent. The response to a strong adverse pressure gradient is a function of Reynolds number[1].

* 名古屋大学工学部

The difficulty in predicting transonic flows is caused by the existence of non-linear phenomena. Hence the flow equation must be represented by a non-linear equation. The basic equation which represents most fluid dynamics of interest is the Navier-Stokes Equations. By neglecting the least significant part under certain physical considerations, an approximation to the governing equations can be developed.

The numerical solution of the Navier-Stokes equations for aerodynamic predictions is now made possible as a result of increases in computer capability and advances in grid generation techniques[2].

Algebraic eddy viscosity models are still the most common choice for turbulent compressible Navier-Stokes equations. These models are quite acceptable for the turbulence modeling of attached turbulent boundary layer without shock waves[4].

Baldwin and Lomax[5] proposed an algebraic

eddy viscosity, patterned after Cebeci and Smith[6], which is intended for separated turbulent flows. In this model, the determination of the boundary layer edge is not required, and thus eliminates a source of potential error of the computed eddy viscosity in the outer layer.

Several further evaluations on the model proposed some modifications either on parameters[7] used or on the way how an abritrary function is defined[8].

On the other hand, Stock and Haase[9], proposed a slightly different formulation of the outer eddy viscosity. In their proposal, a boundary layer edge can be determined by using the function defined in the Baldwin-Lomax model. However, the displacement thickness, which will be later used to calculate the eddy viscosity equation, is derived from Coles velocity profile in defect form[10].

Described here are the results of a series of computations using two algebraic eddy viscosity formulations to simulate transonic flows over NACA-0012 airfoil. The flows under consideration are unsteady compressible at $M_\infty = 0.8$ and $Re = 10^6$. The Yee-Harten scheme is employed to ensure the non-oscillatory approximation to shocks and other contact discontinuities.

In attempt to have an insight and understanding into the physics of the transonic flow characteristics around the considered airfoil, the results are compared with the experiment which was conducted in our transonic tunnel at Nagoya University. In section 2, brief outlines of the governing equations, the numerical scheme and the turbulence models used in this study will be presented. The results will be shown in section 3.

2. METHOD OF CALCULATION

2.1 Governing Equations

The basic equations under study are the Navier Stokes Equations. Considering the efficient numerical process, an approximation to the governing equations can be developed. One of such approximations is the Thin Layer Navier-Stokes equations. The diffusion process along the body surface is neglected[5], while the normal component of the momentum equation is retained, unlike the conventional Boundary Layer approximation. The two dimensional Thin Layer Navier Stokes Equations in Cartesian coordinates can be written in the conservation form:

$$Q_t + F_x + G_y = S_y \tag{1}$$

where

$$Q = \begin{bmatrix} \rho \\ \rho u \\ \rho v \\ e \end{bmatrix}, \quad F = \begin{bmatrix} \rho u \\ \rho u^2 + p \\ \rho uv \\ (e+p)u \end{bmatrix}, \quad G = \begin{bmatrix} \rho v \\ \rho uv \\ \rho v^2 + p \\ (e+p)v \end{bmatrix}$$

$$S = \begin{bmatrix} 0 \\ \tau_{xy} \\ \tau_{yy} \\ u\tau_{xy} + v\tau_{yy} + q_y \end{bmatrix}$$

$$p = (\gamma - 1)\left\{ e - \frac{1}{2}\rho(u^2 + v^2) \right\}, \quad T = \frac{p}{(\gamma - 1)\rho}$$

The variables ρ, u, v, p, e and T are made non-dimensional by the following reference values: density $\bar{\rho}_\infty$, velocity component $\bar{U}_\infty$, pressure $(\bar{\rho}_\infty \bar{U}_\infty)$, total energy per unit volume $(\bar{\rho}\bar{U}_\infty^2)$ and temperature $\bar{T}_\infty$, respectively. The bar denotes dimensional quantities. Finally, μ is the dimensionless dynamic viscosity defined as $\bar{\mu}/\bar{\mu}_\infty$. For the evaluation of μ, the Sutherland's formula is employed. In the dimensionless form:

$$\mu = \frac{1+C}{T+C} T^{3/2}, \text{ where } C = \frac{110.4}{T_\infty} \tag{2}$$

In the present study, T_∞ is assumed 300 K. The dimensionless heat conduction k is defined as $k = \gamma\mu/Pr$ (Prandtl number $Pr = 0.72$).

Avoiding difficulties in the irregular shape of physical domain, equation (1) is transformed into the curvilinear coordinates of computational domain using the following relation

$$\xi = \xi(x, y), \quad \eta = \eta(x, y) \tag{3}$$

While maintaining the strong conservation property, equation (1) can be written in generalized coordinates,

$$\hat{Q}_\tau + \hat{F}_\xi + \hat{G}_\eta = \frac{1}{Re} S_\eta \tag{4}$$

where

$$\hat{Q} = J^{-1} Q,\ \hat{F} = J^{-1}(\xi_x F + \xi_y G),$$
$$\hat{G} = J^{-1}(\eta_x F + \eta_y G),$$
$$\hat{S} = \frac{\mu}{J} \begin{bmatrix} 0 \\ \omega^2 u_u + \vartheta \eta_x \\ \omega^2 v_\eta + \vartheta \eta_y \\ \omega^2 \left\{ \frac{1}{2}(u^2 + v^2) + kT_\eta \right\} + \vartheta \phi \end{bmatrix}$$

with

$$\omega^2 = \eta_x^2 + \eta_y^2,\ \vartheta = \frac{1}{3}(\eta_x u_\eta + \eta_y v_\eta),$$
$$\phi = (\eta_x u + \eta_y v)$$

$J = \xi_x \eta_y - \xi_y \eta_x$ is the Jacobian.

Jacobian matrices are defined as $A = \partial F(Q)/\partial Q$ and $B = \partial G(Q)/\partial Q$, and the Jacobian matrices in generalized coordinates are written as:

$$\hat{A} = (\xi_x A + \xi_y B) \text{ and } \hat{B} = (\eta_x A + \eta_y B) \tag{5}$$

Finally, the diagonalization of eq. 5 is obtained by using R_ξ and R_η matrices whose columns are eigen vectors of $\hat{A}$ and $\hat{B}$, in the following:

$$R_\xi^{-1} \hat{A} R_\xi = A_\xi \text{ and } R_\eta^{-1} \hat{B} R_\eta = B_\eta \tag{6}$$

Matrices R_ξ^{-1} and R_ξ as well as R_η^{-1} and R_η employed in this study can be seen in the Appendix.

2.2 Numerical Scheme

In this section a numerical method with the Yee-Harten TVD scheme will be briefly outlined. More details of the method can be found in ref. 1). Considering the procedure to explicitly solve the viscous term on the right hand side of eq. 4, we only have to solve the left hand side of the equations. A one parameter family of TVD scheme for solving the left hand side of eq. (4) by the implicit backward Euler method is

$$\hat{Q}_{i,k}^{n+1} + \lambda_\xi (\tilde{F}_{i+\frac{1}{2},k}^{n+1} - \tilde{F}_{i-\frac{1}{2},k}^{n+1}) + \lambda_\eta (\tilde{G}_{i,k+\frac{1}{2}}^{m+1} - \tilde{G}_{i,k-\frac{1}{2}}^{m+1}) = \hat{Q}^n \tag{7}$$

where $\lambda^\xi = \frac{\Delta t}{\Delta \xi}$ and $\lambda^\eta = \frac{\Delta t}{\Delta \eta}$. $\Delta\xi$ and $\Delta\eta$ denote the grid spacings in the ξ and η direction. In this study, $\hat{Q}_{i+\frac{1}{2},k}$ is calculated as the Roe's symmetric average:

$$\hat{Q}_{i+\frac{1}{2}} = \frac{\left(\sqrt{\frac{\rho_{i+1}}{\rho_i}}\,\hat{Q}_{i+1} + \hat{Q}_i\right)}{\left(\sqrt{\frac{\rho_{i+1}}{\rho_i}} + 1\right)} \tag{8}$$

The flux function $\tilde{F}_{i+\frac{1}{2},k}$ is expressed as

$$\tilde{F}_{i+\frac{1}{2},k} = \frac{1}{2}(\hat{F}_{i,k} + \hat{F}_{i+1,k} + R_{i+\frac{1}{2}} \Phi_{i+\frac{1}{2}}) \tag{9}$$

If the eigen values of $\hat{A}$ and $\hat{B}$ can be expressed as

$$(a_\xi^1, a_\xi^2, \ldots, a_\xi^m) \text{ and } (a_\eta^1, a_\eta^2, \ldots, a_\eta^m) \tag{10}$$

Then, the l-th component $\Phi_{i+\frac{1}{2}}^l$, where $l = 1, 2, \ldots, m$ is written as

$$\Phi_{i+\frac{1}{2}}^l = \frac{1}{2}\psi(a_{i+\frac{1}{2}}^l)(g_i^l + g_{i+1}^l) - \psi(a_{i+\frac{1}{2}}^l + \gamma_{i+\frac{1}{2}}^l)\alpha_{i+\frac{1}{2}}^l \tag{11}$$

Here α^l is the difference of the characteristic variables in the local direction, and is defined as

$$\alpha_{i+\frac{1}{2}} = R_{i+\frac{1}{2}}^{-1} \frac{Q_{i+1,k} - Q_{i,k}}{0.5*(J_{i+1,k} + J_{i,k})} \tag{12}$$

and

$$g_i^l = S \cdot max\,(0, min\,(|\alpha_{i+\frac{1}{2}}^l|, S \cdot \alpha_{i+\frac{1}{2}}^l))$$
$$S = Sign\,(\alpha_{i+\frac{1}{2}}^l) \tag{13}$$

$$\psi(z) = \begin{cases} |z| & |z| \geq \epsilon \\ \frac{(z^2+\epsilon^2)}{2\epsilon} & |z| < \epsilon \end{cases} \tag{14}$$

with

$$\gamma_{i+\frac{1}{2}} = \frac{1}{2}\psi(a_{i+\frac{1}{2}}^l) \begin{cases} \frac{(g_i^l + g_{i+1}^l)}{\alpha_{i+\frac{1}{2}}^l} & \alpha \neq 0 \\ 0 & \alpha = 0 \end{cases} \tag{15}$$

Another numerical flux $\tilde{G}_{i,k+\frac{1}{2}}$ can be defined similarly.

For efficiency of computation a linearized conservation form has been intentionally chosen to keep the strong conservation property. Finally, an ADI form of the linearized implicit algorithm has been constructed.

2.3 Grid and Boundary Condition

An algebraically generated C grid is used here in this study. To calculate the flow, 201 X 30 mesh is employed, with no special clustering near the shock. Figure 1 shows the grid distribution around the airfoil, with 120 grid points on the airfoil surface. The outer boundary is 10 chord lengths away from the body.

The simulation for each case is initially started with a uniform free stream at the prescribed Mach number. At the outer boundary the flow is assumed uniform with the free stream: $u = U_\infty$ and $v = 0$. At the downstream boundary, non-gradients of flow variables are applied ($\frac{\partial \phi}{\partial x} \equiv 0$), except for pressure. Regarding to the pressure, the same value as the upstream flow was enforced on the boundary. The surface of the airfoil is impermeable, and "no-slip" boundary condition is employed for the viscous case. In the case of the Euler equations, a "slip" boundary condition is imposed and the tangential velocity at the wall is linearly extrapolated from the value next to the wall. The pressure on the body surface is calculated from the normal momentum equation. The total enthalpy is held constant along the body, which is the same value as the free stream. Along the wake cut, each quantity is calculated by averaging the variables above and below the cut.

The parameter ϵ included in Eq. (12) is set equal to 0.2 for all cases. The result of using other values showed no significant differences.

To simulate the separation at boundary layer which is likely to occur in the transonic flow, the grid is refined up to the viscous sublayer scale. ΔY_{min} of the first spacing is 4×10^{-4} which is fully in the range of the thickness of boundary layer in incompressible flow.

2.4 Turbulence Model

2.4.1 Baldown and Lomax (BLM)

This is a two layer model in which an eddy viscosity is separately calculated for inner and outer region. The inner region follows the Prandtl-Van Driest formulation. The distribution of vorticity is used to determine the length scale, thereby avoiding of finding the outer edge of the boundary layer. For inner region:

$$(\mu_t)_{inner} = \rho l^2 |\omega| \tag{16}$$

where

$$l = ky \left\{1 - exp(-y^+/A^+)\right\},$$

$$y^+ = \frac{\rho_w u_\tau y}{\mu_w}, u_\tau = \sqrt{\frac{\tau_w}{\rho_w}} \tag{17}$$

k is von Kàrmàn constant = 0.4 and $A^+ = 26$. $|\omega|$ is the absolute magnitude of vorticity. The eddy viscosity for the outer region is given by:

$$(\mu_t)_{outer} = KC_{cp}\rho F_{wake} F_{Kleb}(y) \tag{18}$$

where

$$F_{wake} = \left\{ \begin{array}{l} y_{max} F_{max} \\ \dfrac{C_{wk} y_{max} U^2_{dif}}{F_{max}} \end{array} \right\} \text{the smaller} \tag{19}$$

The constants $C_{cp} = 1.6$, $K = 0.0168$ and $C_{wk} = 0.25$ are defined due to the Cebeci-Smith[6] formulation for contant pressure boundary layer at transonic speed. The quantities y_{max} and F_{max} are determined from the function

$$F(y) = y|\omega| \left\{1 - exp(\frac{-y^+}{A^+})\right\} \tag{20}$$

F_{max} is the maximum value of F(y) along the y-coordinate, and y_{max} is the location where it occurs. U_{dif} is the difference between maximum and minimum velocity in profile. The function $F_{Kleb}(y)$ is the Klebanoff intermittency factor defined as

$$F_{Kleb}(y) = \left\{1 + 5.5 (\frac{C_{kl} y}{y_{max}})^6\right\}^{-1} \tag{21}$$

with $C_{kl} = 0.3$.

2.4.2 Stock and Haase Model (SHM)

The Stock and Haase model (SHM) is almost the same model as the BLM. However, another procedure to evaluate the turbulent length scale is proposed, which enables the direct application of Cebeci-Smith's eddy viscosity formulation.

For the outer region, Cebeci-Smith's eddy viscosity is given by:

$$(\mu_t)_{outer} = kpU_e\delta^* F_{Kleb}(y) \qquad (22)$$

Where U_e is the velocity at the edge of the boundary layer.

The Klebanoff intermittent factor is defined as

$$F_{Kleb}(y) = \left\{ 1 + 5.5 \left(\frac{y}{\delta}\right)^6 \right\}^{-1} \qquad (23)$$

where δ is the boundary layer edge.

If the Coles formulation which consists of a summation of the law of the wall and the wake can be written as

$$y \left|\frac{\partial U}{\partial y}\right| = \frac{U_e}{k} \left[\pi|\sigma|\Pi\frac{y}{\delta}\sin\left(\pi\frac{y}{\delta}\right) + \sigma\right] \qquad (24)$$

where Π is Coles pressure gradient parameter.

The maximum of the property $y\left|\frac{\partial U}{\partial y}\right|$ will provide

$$\delta = 1.548 y_{max} \qquad (25)$$

The results of numerically experimental velocity profiles show that by increasing the constant parameter in Eq. (25) by 25%

$$\delta = 1.936 y_{max} \qquad (26)$$

the viscous-layer thickness was predicted well[9]. The displacement thickness δ^* is evaluated by numerically integrating the velocity profiles from $y = 0$ or $y = y_{u=0}$ to δ.

3. RESULT AND DISCUSSION

The transonic flow solutions for NACA0012 airfoil were computed for $Re_\infty = 1 \times 10^6$ and $M_\infty = 0.80$. All computations were carried out up to the time when the mean flow travels by 5.273 chord length.

The calculated result was considered a steady state when the relative error for every flow variables become less than 10^{-4}. Each case converged at about 850 steps. It required 110 second CPU time on Fujitsu FACOM VP200.

Turbulent eddy viscosities are used in the BLM and SHM. These are made non-dimensional by the free steam molecular viscosity μ_∞ and plotted in the y-coordinate in Figs. 2 and 3. Both

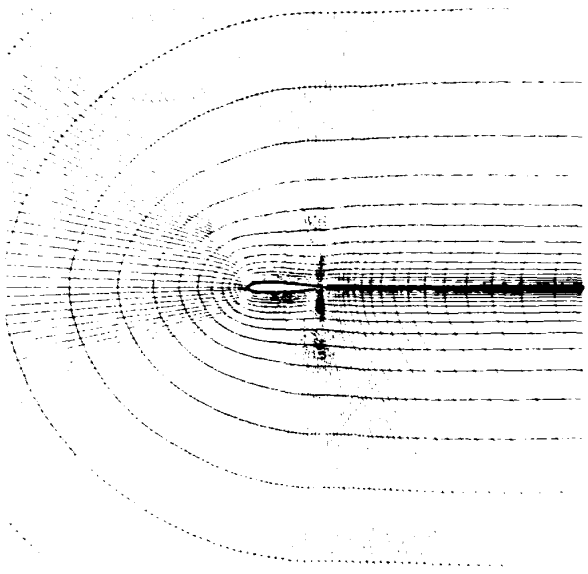

Fig. 1. 201 X 30 "C" Grid for NACA-0012 Airfoil

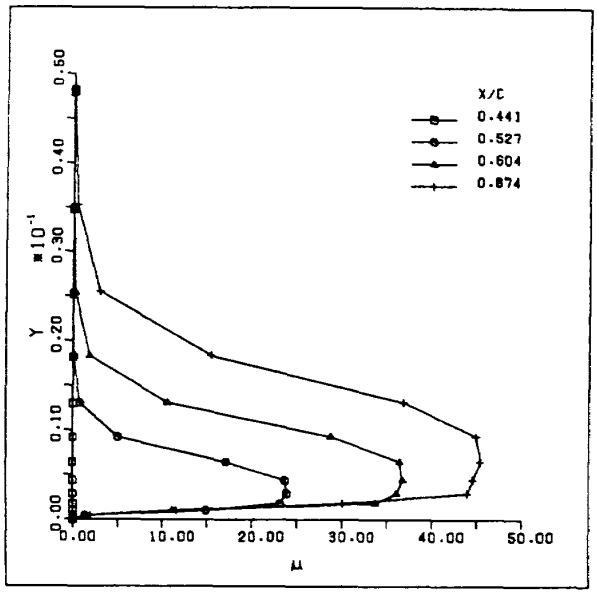

Fig. 2. Turbulent Viscosity Profiles (BLM): $M_\infty = 0.8$, $\alpha = 0$ and $Re = 1 \times 10^6$.

models produce almost the same profiles with rather flat peaks which go to zero outside the boundary layer.

As described in ref.[9] the eddy viscosity calculated by the BLM is higher than that by the SHM. The profiles μ_t indicate a gradual change. A comparison of mean velocity profiles is made at the same station between the solutions using both models and the laminar one in Fig. 4. In a laminar flow, a very large region of reverse flow is observed. This seems to be natural, since

the laminar viscous flows produce a very thin layer. Thus easily initiated a separation in further upstream. The adverse pressure gradient then boosts up the reverse flow.

Inserting the turbulence model into the equations means to bring the flow in outer region with higher energy to the closer area to the wall. The higher the eddy viscosity becomes, the less likely a reverse flow is to occur. The higher value of eddy viscosity in the BLM solution can be seen from Fig. 4, which has eliminated the possibility of reverse flow at the surface. The eddy viscosity by the SHM, which is slightly smaller than that by the BLM, retains the reverse flow around the shock region.

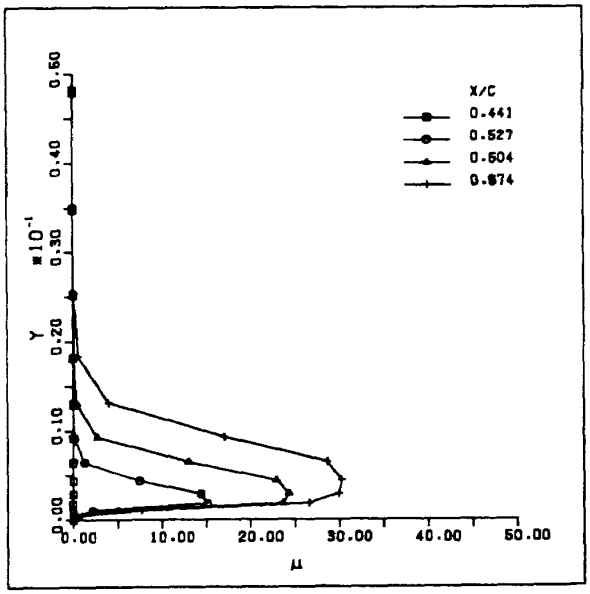

Fig. 3. Turbulent Viscosity Profiles (SHM): $M_\infty = 0.8$, $\alpha = 0$ and $Re = 1 \times 10^6$.

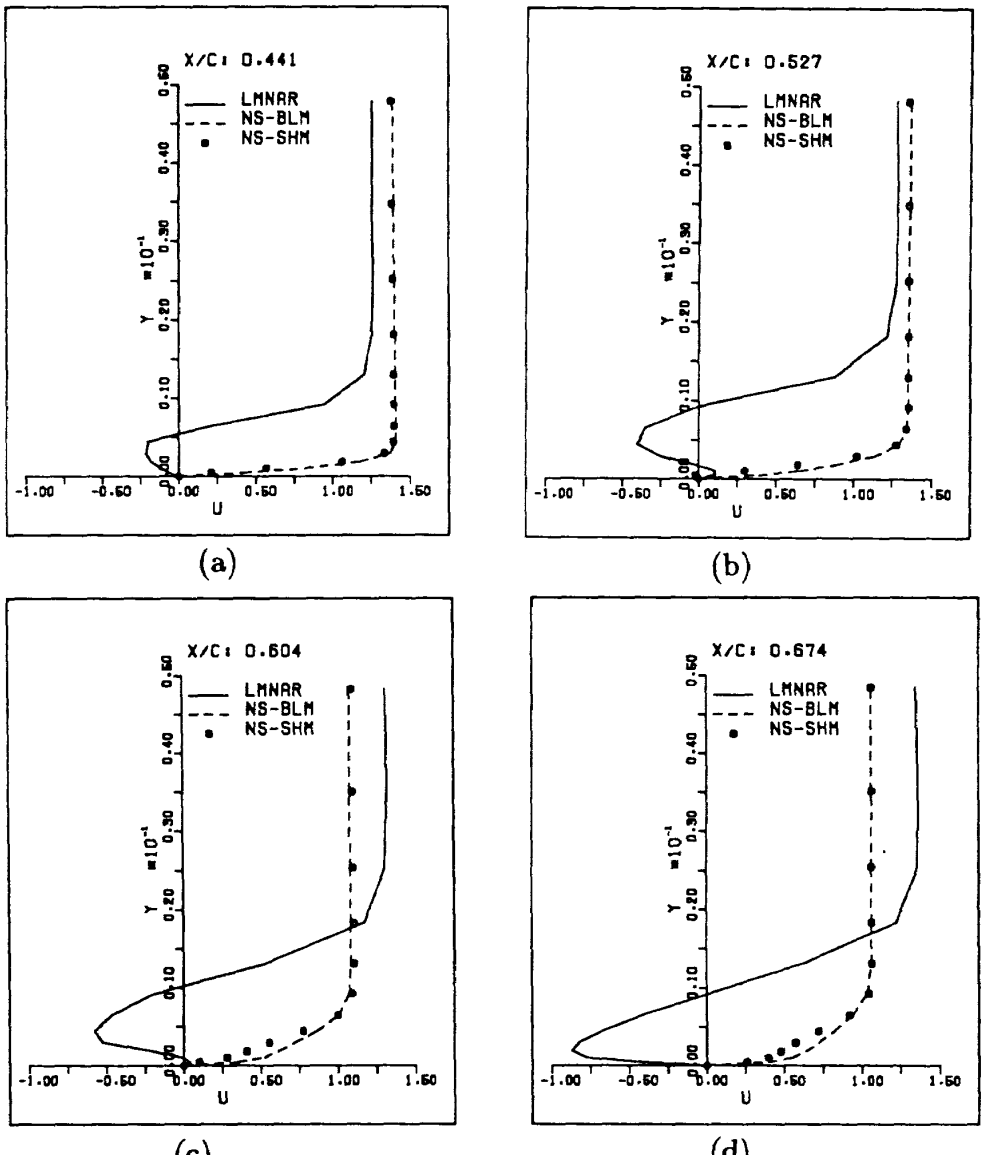

Fig. 4. Mean Velocity Profiles: $M_\infty = 0.8$, $\alpha = 0$ and $Re = 1 \times 10^6$
a) x/c = 0.441 b) x/c = 0.527 c) x/c = 0.604 d) x/c = 0.674

A comparison with experiment for wall pressure distribution can be seen in Fig. 5. Two computed distributions are included. One of these computed data is an inviscid calculation and another one was obtained by using eddy viscosity of the BLM. The experimental data seems to be rather higher as compared with both numerical results. This might be due to the fact

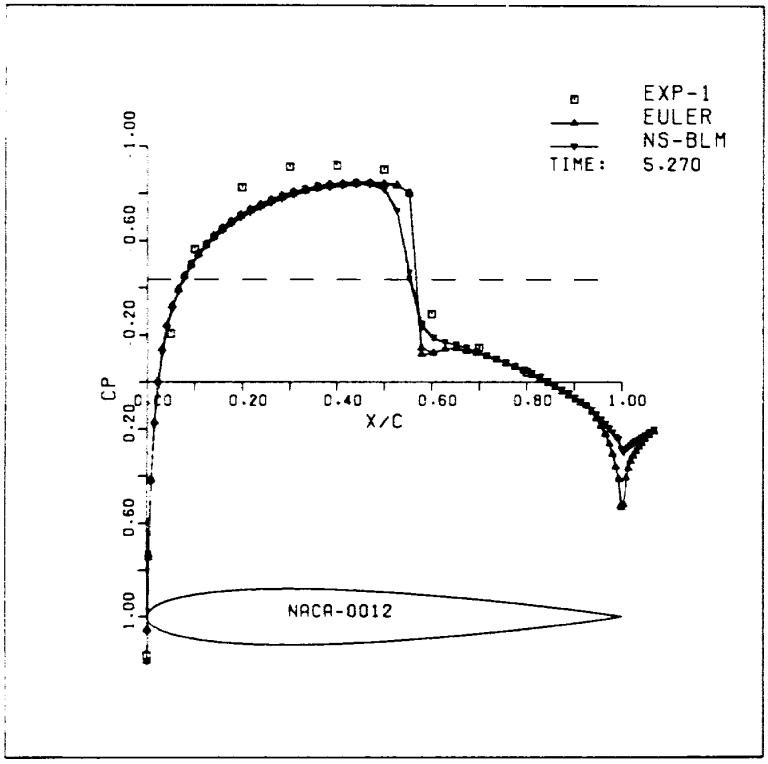

Fig. 5. Surface Pressure Distribution:
$M_\infty = 0.8$, $\alpha = 0$ and $Re = 1 \times 10^6$

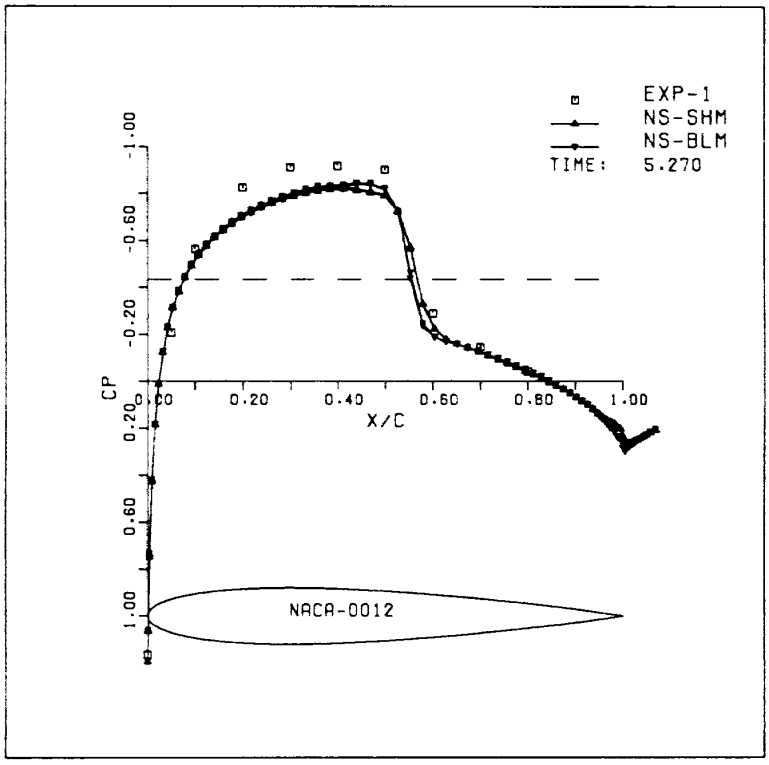

Fig. 6. Surface Pressure Distribution:
$M_\infty = 0.8$, $\alpha = 0$ and $Re = 1 \times 10^6$

that the wall interference effect is not yet included in our experimental data. All comparisons except for what were previously mentioned are in reasonable agreement. The inviscid solution did give a stronger shock: the shock is more upright than the viscous result. Some improvement is seen in the viscous case. However, the level of pressure recovery still underestimated by this method.

Figure 6 shows a comparison of surface pressure distribution between the result predicted by implementing both turbulence models and the experimental data. The calculations are almost identical except in the vicinity of shock location and in the pressure recovery location. As compared with the BLM, the pressure distribution by the SHM is underestimated. The recovery pressure level provided by the SHM seems to have a better agreement with the experiment. The very thin and small reverse flow predicted by SHM might contribute to a better result.

In Fig. 7, the distribution of skin friction along the surface clearly shows the discrepancy of both models. The transition is noted as the skin friction starts to decrease, then followed by a sharp drop at the reverse flow in the shock region. A slow rise of skin friction is observed in the redeveloping region after the shock, then followed by gradually decrease toward the separation in the trailing edge. In the BLM this kind of phenomena is not as sharp as in the SHM. Considering the coincidence of pressure recovery level between the experimental data and the SHM, the flow characteristics: a separation around shock region, followed by redeveloping region, and then another separation near the trailing edge, might be numerically confirmed.

Figure 8 shows the density contours of the viscous and inviscid result. Here, the calculated result is compared with the schlieren picture taken by our experiment. Once again, the shock location is well predicted in all cases.

4. CONCLUSION

Transonic flows ranging from the inviscid to thin layer viscous flow have been simulated numerically in this preliminary study by using the TVD scheme of Euler backward implicit method.

In the viscous case two turbulent models: Baldwin-Lomax (BLM) and Stock-Haase model (SHM) are incorporated into the governing equa-

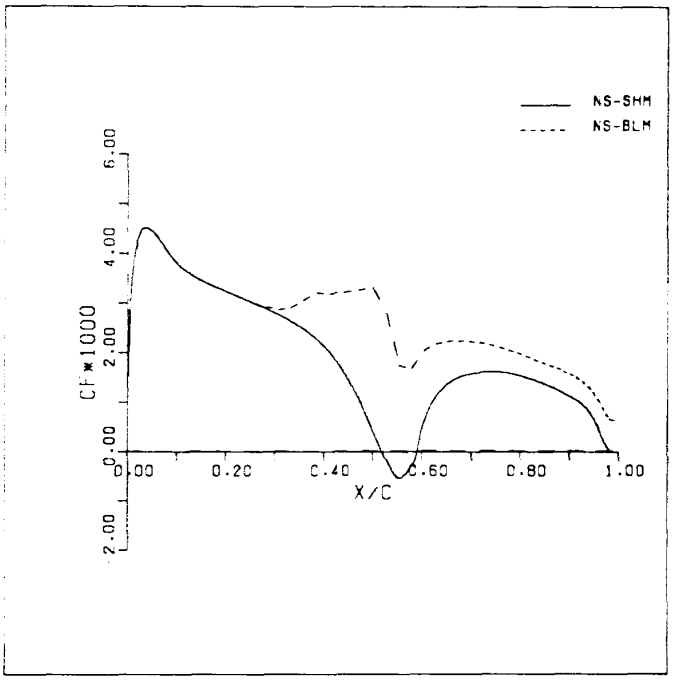

Fig. 7. Skin-friction Distribution:
$M_\infty = 0.8$, $\alpha = 0$ and $Re = 1 \times 10^6$

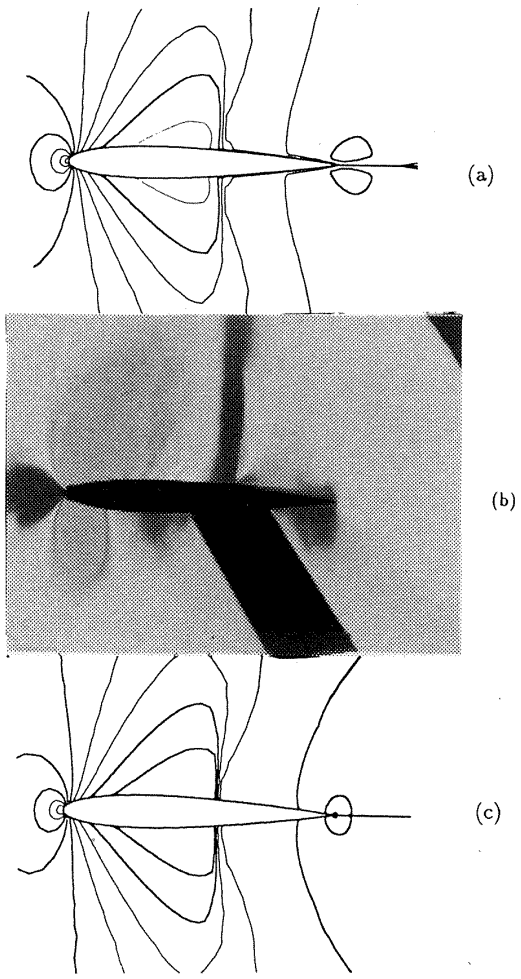

Fig. 8. Density Contours:
$M_\infty = 0.8$, $\alpha = 0$ and $Re = 1 \times 10^6$
a) Euler Eqs. b) Experiment
c) Navier-Stokes Eqs.

tions. As compared with experimental data, the SHM shows a better agreement with the experiment.

No attempt has been yet made in the present study to use more rigorous turbulence model. Since the flow is transonic, even the algebraic turbulence model might be adequate for regions in the vicinity of shock and in the separated flow. The flow separation has not yet been confirmed over the surface of the airfoil by experiment. The flow characteristics about NACA0012 airfoil should be considered qualitative.

REFERENCES

1) Deiwert, G.S., *Numerical Simulation of High Reynolds Number Transonic Flows*, AIAA Journal, Vol. 13, No. 10, Oct. 1975, pp. 1354-1359.
2) Yee, H.C. & Harten, A., *Implicit TVD Scheme for Hyperbolic Conservation Laws in Curvilinear Coordinate*, AIAA Paper 85-1513.
3) Beam, R. and Warming, R., *An Implicit Factored Scheme for the Compressible Navier Stokes Equations*, AIAA Journal, Vol. 16, April 1978, pp. 393-402.
4) Deiwert, G.S., *Computation of Separated Transonic Turbulent Flows*, AIAA Journal, Vol. 14, No. 6, June 1976, pp. 735-740.
5) Baldwin, B. and Lomax, H., *Thin Layer Approximation and Algebraic Model for Separated Turbulent Flows*, AIAA Paper 78-257.
6) Cebeci, T. and Smith, A.M.O., *Analysis of Turbulent Boundary Layers*, Academic Press, 1974.
7) Granville, P.S., *Baldwin-Lomax Factors for Turbulent Boundary Layers in Pressure Gradients*, AIAA Journal, Vol. 25, No. 12, Dec. 1987, pp. 1624-1627.
8) Visbal, M. and Knight, M., *Turbulence Model for Two Dimensional Shock-Wave/ Boundary Layers Interactions*, AIAA Journal, Vol. 22, No. 7, July 1984, pp. 921-928.
9) Stock, H.W. and Haase, W., *Determination of Length Scales in Algebraic Turbulence Models for Navier Stokes Methods*, AIAA Journal, Vol. 27, No. 1, Jan. 1989, pp. 5-14.
10) Hinze, J.O., *Turbulence*, McGraw-Hill, New York, 1959.

APPENDIX

The eigen values and eigenvectors are expressed in term of the generalized metrics n_x and n_y which define the x and y components.

$$\hat{n}_x = n_x/\bar{S} \quad \text{and} \quad \hat{n}_y = n_y/\bar{S} \tag{A-1}$$

where

$$\bar{S} = \sqrt{n_x^2 + n_y^2} \tag{A-2}$$

The eigenvalues of the Jacobian matrix $\partial F/\partial Q$ are defined as

$$\lambda^1 = (\hat{U} - c)S,\ \lambda^2 = \hat{U}S,\ \lambda^3 = (\hat{U} + c)\bar{S},$$
$$\lambda^4 = \hat{U}\bar{S} \tag{A-3}$$

The normalized contravariant velocity is

$$\hat{U} = u\hat{n}_x + v\hat{n}_y \tag{A-4}$$

And for subsequent use, let define

$$\hat{V} = u\hat{n}_x - v\hat{n}_y \tag{A-5}$$

The matrix R^{-1} is given by

$$R^{-1} = \begin{bmatrix} +\frac{\chi}{c}\frac{q^2}{2} + \hat{U} & -\frac{\chi}{c}u - \hat{n}_x & -\frac{\chi}{c}v - \hat{n}_y & +\frac{\chi}{c} \\ -\frac{\chi}{c}\frac{q^2}{2} - \hat{V} + c & +\frac{\chi}{c}u - \hat{n}_y & +\frac{\chi}{c}v + \hat{n}_x & -\frac{\chi}{c} \\ -\frac{\chi}{c}\frac{q^2}{2} + \hat{V} + c & +\frac{\chi}{c}u + \hat{n}_y & +\frac{\chi}{c}v - \hat{n}_x & -\frac{\chi}{c} \\ -\frac{\chi}{c}\frac{q^2}{2} - \hat{U} & -\frac{\chi}{c}u + \hat{n}_y & -\frac{\chi}{c}v + \hat{n}_x & +\frac{\chi}{c} \end{bmatrix} \tag{A-6}$$

and the matrix R of right eigen vectors is given by

$$R = \begin{bmatrix} \frac{1}{c} & \frac{1}{c} & \frac{1}{c} & \frac{1}{c} \\ \frac{u}{c} - \hat{n}_x & \frac{u}{c} - \hat{n}_y & \frac{u}{c} + \hat{n}_x & \frac{u}{c} + \hat{n}_y \\ \frac{v}{c} - \hat{n}_y & \frac{v}{c} + \hat{n}_x & \frac{v}{c} + \hat{n}_y & \frac{v}{c} - \hat{n}_x \\ \frac{q^2}{2c} - \hat{U} + \frac{c}{\chi} & \frac{q^2}{2c} + \hat{V} & \frac{q^2}{2c} - \hat{U} + \frac{c}{\chi} & \frac{q^2}{2c} - \hat{V} \end{bmatrix} \tag{A-7}$$

In the above, $\chi = \gamma - 1$.